Journal of Magnetism and Magnetic Materials 419 (2016) 580–587

Contents lists available at ScienceDirect

Journal of Magnetism and Magnetic Materials

journal homepage: www.elsevier.com/locate/jmmm

Quantitative study of FORC diagrams in thermally corrected Stoner– Wohlfarth nanoparticles systems

E. De Biasi *, J. Curiale, R.D. Zysler

CNEA, CONICET, Centro Atómico Bariloche, Av. Bustillo 9500, 8400 S. C. de Bariloche, Río Negro, Argentina.

ARTICLE INFO

Article history:
Received 24 June 2015
Received in revised form
16 June 2016
Accepted 25 June 2016
Available online 27 June 2016

Keywords:
FORC
Nanoparticles
Anisotropy distribution
Interaction field distribution
FORC profiles distributions
Stoner– Wohlfarth system

ABSTRACT

The use of FORC diagrams is becoming increasingly popular among researchers devoted to magnetism and magnetic materials. However, a thorough interpretation of this kind of diagrams, in order to achieve quantitative information, requires an appropriate model of the studied system. For that reason most of the FORC studies are used for a qualitative analysis. In magnetic systems thermal fluctuations "blur" the signatures of the anisotropy, volume and particle interactions distributions, therefore thermal effects in nanoparticles systems conspire against a proper interpretation and analysis of these diagrams. Motivated by this fact, we have quantitatively studied the degree of accuracy of the information extracted from FORC diagrams for the special case of single-domain thermal corrected Stoner– Wohlfarth (easy axes along the external field orientation) nanoparticles systems. In this work, the starting point is an analytical model that describes the behavior of a magnetic nanoparticles system as a function of field, anisotropy, temperature and measurement time. In order to study the quantitative degree of accuracy of our model, we built FORC diagrams for different archetypical cases of magnetic nanoparticles. Our results show that from the quantitative information obtained from the diagrams, under the hypotheses of the proposed model, is possible to recover the features of the original system with accuracy above 95%. This accuracy is improved at low temperatures and also it is possible to access to the anisotropy distribution directly from the FORC coercive field profile. Indeed, our simulations predict that the volume distribution plays a secondary role being the mean value and its deviation the only important parameters. Therefore it is possible to obtain an accurate result for the inversion and interaction fields despite the features of the volume distribution.

1. Introduction

The use of FORC diagrams became a frequently used tool to study different kind of magnetic systems [1–12]. As this method provides more information than conventional hysteresis cycles from the same type of experiment, its use has been increased considerably in recent years. However, its analysis and interpretation in order to obtain quantitative information is not straightforward and requires, in many cases, the use of models to understand the results [13]. The nanoparticles "universe" does not escape to this reality, and the difficulty increases due to the fact that the experimental results usually strongly depend on temperature [14].

The need to know the magnetic properties of nanostructured systems is becoming important because these parameters determine the behavior and magnetic relaxation of the magnetization, essential in applications, e.g., the use of nanoparticles in hyperthermia [15,16]. In this case, the magnetic relaxation channels are strongly determined by the distribution of anisotropy energies as well as interactions between particles. In high-density magnetic data storage [12,17,18], the knowledge of switching fields distribution and interactions between magnetic grains are essential to optimize the storage process. The temporal stability of the stored information and the maximum speed for the read/write process depends on the above-mentioned distributions. To access, quantitatively to the switching field and interaction distributions from minor hysteresis loops is not straightforward. Since the pioneer work of Preisach [19], many theoretical efforts have been made to understand the validity range and the physics behind FORC diagrams [17,20–24].

Motivated by the above-mentioned ideas, the main achievement of this work is to study the degree of accuracy of the quantitative information, which is possible to obtain from FORC diagrams, about the switching field distribution and interactions in nanoparticle systems. As starting point, we used a model [25]

* Corresponding author.
E-mail address: debiasi@cab.cnea.gov.ar (E. De Biasi).

http://dx.doi.org/10.1016/j.jmmm.2016.06.075
0304-8853/

that describes the behavior of the magnetization of an interacting nanoparticle system with size, anisotropy, and interaction field distributions, to obtain an analytical expression for the FORC density. We assume that the particles ease axes are oriented along the external magnetic field direction (Stoner– Wohlfarth model) and the interactions fields are not dependent of the magnetic state of the nanoparticle ensemble. Numerical simulations allow us to study the degree of accuracy achieved when original information is recovered from the simulated FORC diagrams.

2. The model

In this work we developed a model to build FORC diagrams based on the results of a previous work [25] where thermal effects have been included on the classical Stoner– Wohlfarth model. On that case it was assumed non-interacting particles having a uniaxial effective anisotropy and the magnetic relaxation is governed by the Arrhenius law, being the magnetization reversal time given by the Master Equation. In order to deal with interactions, we upgraded the above-mentioned model redefining the effective field acting on each nanoparticle including interactions in the same way as in the Preisach model.

The evolution of the magnetization M, Eq. (1), is given by two contributions. The first term corresponds to the fraction of particles that are in the superparamagnetic regime, and the second term corresponds to the blocked fraction. $L\left(\tilde{H},T,\tau_m\right)$ is the probability to find the system in the superparamagnetic regime, where $\tilde{H}$ is the total effective magnetic field acting on each nanoparticle, T is the temperature and τ_m the temporal windows of the experiment. Finally, the total effective magnetic field, $\tilde{H}=H+H_i$, is given by the interaction (H_i) and the external applied ($\mathbf{H}$) fields.

$$M(H,T,\tau_m) = \langle M\left(\tilde{H},T,\tau_m\right)\rangle_{SP} L\left(\tilde{H},T,\tau_m\right) + \left[1 - L\left(\tilde{H},T,\tau_m\right)\right]\left[\langle M_0\rangle_B P_0 + \langle M_1\rangle_B P_1\right] \quad (1)$$

The contribution of the blocked population to the total magnetization is a function of P_0, P_1 which correspond to the fraction of particles whose magnetic moments are oriented along the direction given by the first and second energy minima E_0 and E_1 respectively. M_0 and M_1 are the magnetization values corresponding to the minima orientations projected on the $\vec{H}$ direction, and the brackets indicate the statistical average of the magnetization around each energy minimum. The statistical average of the superparamagnetic contribution must be performed over the full space of the magnetization coordinates.

The probability of finding a particle in the superparamagnetic regime is given by:

$$L(H,T,\tau_m)=1-\gamma(H,T,\tau_m)$$
$$\gamma(H,T,\tau_m) = e^{-\tau_m/\tau^*} \quad (2)$$

where τ^* is the effective time of passage of the magnetization from a minimum to the other.

It is necessary to remark that the use of this model require the knowledge of the time evolutions of the population P_0 and P_1. The Eq. (3) gives us such evolution as a function of the time τ_m (small enough as well as τ^* remain constant while the external field is change between successively measurements).

$$P_0(t+\tau_m) = P_0(t) + L(H,T,\tau_m)\left[P_0^{\infty} - P_0(t)\right]$$
$$P_0 + P_1 = 1 \quad (3)$$

P_0^{∞} is the equilibrium population associated to the E_0 energy minimum. (Eqs. (2) and 3) were obtained from the combination of Master Equation and the Arrhenius law.

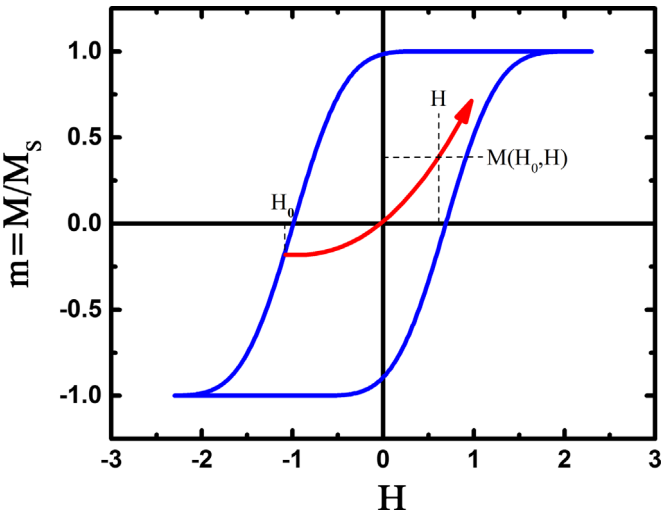

Fig. 1. Schematic illustration of $M(H_0,H)$. The sample is saturated with $H>0$ and then the field is reversed until H_0. The field is reversed again until de desired field H. The magnetization achieved is $M(H_0,H)$.

2.1. Modeling the FORC diagrams

To obtain a set of first order reversal curves, one of which is shown in the schematic Fig. 1, the measurement protocol starts at high value of H (H_{Max}) with the magnetization in thermal equilibrium (therefore it is only a function of T and H_{Max}). The external magnetic field is swept down until a reversal field H_0. The FORC method consists in the measurement of the magnetization as a function of the external magnetic field when it is increased from H_0 back up to H_{Max}. The total magnetization of the system at the applied field H on the FORC with reversal point H_0 is denoted by $M(H_0,H)$, with $H\geq H_0$. A FORC distribution is defined as the mixed second derivative [24]:

$$\rho(H_0,H)=-\frac{\partial^2 M(H_0,H)}{\partial H_0 \partial H} \quad (4)$$

and the FORC diagram is the contour plot of this distribution.

2.1.1. Additional hypotheses

The (Eqs. (1)–3) provide us a way to calculate the ρ distribution. However, it is necessary consider some extra hypothesis in order to get an analytical expression for the calculation of the FORC distribution. *First, the easy axes are aligned along the external magnetic field direction.* This strongly simplifies the problem because the Stoner– Wohlfarth model has analytical solution in that case. Indeed this hypothesis is widely used in the literature of the FORC physics. Even from the beginning of the FORC distribution studies, most of the authors use as building blocks square like loops called hysterons. These entities could be straightforward identified with the parallel configuration of the Stoner– Wohlfarth model.

The second hypothesis assumes the FORC distribution is obtained at low temperature. Particularly the system is not only blocked if not that thermal energy (K_BT) is smaller than the barrier energy ($E_B=KV$ where K is the anisotropy constant and V the volume of the particle). Actually, this hypothesis does not mean an extra restriction because, as it is well known, the magnetic system must be blocked in order to observe a hysteretic behavior and, in consequence, make sense "build" a FORC diagram.

Based on this last hypothesis we can neglect the effect of thermal fluctuations of the magnetization orientation in each energy minima. It means that, as the modulus of the magnetization do not change with thermal fluctuations, in the blocked regime it

is only possible to obtain two discrete values of the magnetization. Then, we can assume that the role of thermal fluctuations are reduced exclusively to assist the reverse of the magnetization passing from a given minimum energy orientation to the other one. Based on the same hypothesis, the γ function of Eq. (3) behaves as:

$$\gamma(H) \approx \theta(H_c - |H|) \tag{5}$$

where H_c is the coercive field corresponding to a given value of K and T, where $\theta(x)$ is the Heaviside step function.

Considering all previous assumptions, and also that the equilibrium population P_0^{∞} (see Eq. 3) can be approximated by a step distribution we obtain an expression for the evolution of the minimum energy population E_0 as:

$$P_0(H, H_0)=1+\gamma(H)\left[\gamma(H_0)-1\right] \tag{6}$$

In this context, using (Eqs. (1)–6) it is possible to obtain the following analytical expression for the FORC distribution, ρ:

$$\rho^{\phi,K,H_i}(H, H_0)= -4\gamma(\tilde{H})\frac{\partial\gamma(\tilde{H})}{\partial H}\frac{\partial\gamma(\tilde{H}_0)}{\partial H_0} \tag{7}$$

where the total magnetic field acting over each particle can be writing as: $\tilde{H}=H+H_i$, being H_i the total interaction field over the particle *i*. This fact completes the model including the last hypothesis: the interaction field acting over a given particle is independent of the magnetic state. We want make some considerations about the way in which the interparticle interactions are added in the model. As in the Presiach like model, we are using the concept of interaction field distribution. However, despite this concept does not has a physical reality; the goal of our work is study the accuracy of the information about the coercive and interactions field's distributions, assuming the validity of the proposed model. Clearly, in a real magnetic nanoparticle system, the interactions are dependent of the magnetic state of the particles. In this sense, when a FORC diagram is built from the experimental data, the image of the coercivity and the interactions fields as disassociated entities in general must be modified. It is not our purpose study this topic, because for each particular case it is necessary dispose of an adequate model that describes the mechanism that governs the magnetization inversion. In this sense, the present treatment could be considered as a first step for further developments.

It is important to remark that the Eq. (7) corresponds to the contribution of only one particle of diameter ϕ, anisotropy K, and interaction field H_i. In order to obtain the distribution of the full ensemble of particles ρ, it is necessary to integrate over the distributions of size (f_ϕ), anisotropy (f_K), and interaction fields (f_{H_i}).

Then, the expression for the FORC distribution of the ensemble is given by:

$$\rho(H,H_0) = \frac{1}{<V>}\int_{\Omega\phi}\phi^3 f_\phi\left\{\int_{\Omega K} f_K\left[\int_{\Omega H_i}\left(\rho^{\phi,K,H_i}\right)f_{H_i}dH_i\right]\mathrm{dK}\right\}d\phi \tag{8}$$

where $<V>$ is the mean volume value and the integrals are performed over the full domain of each parameter (Ω_i, Ω_K ,and Ω_{H_i}). It is useful to note that, as H_i do not depend on the magnetization, after a suitable change of coordinates, we will be able to factorize this equation.

Usually, in the literature the FORC diagrams are expressed in terms of the new coordinates $\tilde{H}_c = (H-H_0)/2$ and $\tilde{H}_u = (H+H_0)/2$ [23,24,26].

In this coordinate system, it is possible to identify:

$$\delta(\tilde{H}_c - H_c)\longleftrightarrow\frac{\partial\gamma(\tilde{H}_c)}{\partial H}$$
$$\delta(\tilde{H}_u + H_i) = \delta(H^* - H_c) \leftrightarrow \frac{\partial\gamma(H^*)}{\partial H} \tag{9}$$

where $H^* = \tilde{H}_u + H_i + H_c$ and H_c is the coercive field for a particle, which is given by:

$$H_c = H_A\left(1 - \sqrt{k_BT\,\log(4\tau_m/\tau_0)/KV}\right) \tag{10}$$

here k_BT is the thermal energy, $H_A = 2K/M_s$ is the anisotropy field, KV is the energy barrier of the particle of volume V, τ_m is the temporal windows of the measurement and τ_0 is the characteristic time relaxation at $T \to \infty$.

It is convenient to note that the derivative of the gamma function on the second line of Eq. (9) must be evaluated in H^* despite the graph is plotted in $(\tilde{H}_c, \tilde{H}_u)$ coordinates.

Substituting Eq. (7) in (8) and tacking into account Eq. (9). $\delta(\tilde{H}_u + H_i)=\delta(H^* - H_c) \leftrightarrow \frac{\partial\gamma(H^*)}{\partial H}$, it is possible to factorize the H_i integral of Eq. (8), despite of γ is function of V and K through τ^*, which leads to the following expression:

$$\rho(\tilde{H}_c, \tilde{H}_u)=-\left\{\int_{\Omega K} f_K\int_{\Omega\phi} f_\phi\frac{4\phi^3}{<V>}\gamma(\tilde{H}_c)\frac{\partial\gamma(\tilde{H}_c)}{\partial H}dKd\phi\right\}$$
$$\left\{\int_{\Omega H_i} f_{H_i}\frac{\partial\gamma(H^*)}{\partial H}dH_i\right\} \tag{11}$$

Then, in this case we can deal with an expression much more simple than the Eq. (8), which also requires less computational effort and evidences an underlying symmetry.

Indeed, this symmetry is given by the fact that there is a proportionality factor between two different profiles of FORC distribution at constant $\tilde{H}_u$. This factor is the H_i integral in the Eq. (11), which account for the interaction field's distribution. Despite we start our treatment form a model described in reference [25], by the simplifications derived from the hypotheses on 2.1.1, we believe that the resulting model synthetized in Eq. (11) are compatible with the Presisach–Néel model [27,28].

Then, from the Eq. (11) it is evident that the information about the H_c and H_i distributions are provided by the FORC diagram in the $\tilde{H}_c$ and $\tilde{H}_u$ axis. This affirmation could also be valid even in Eq. (8) using the appropriate coordinates.

2.2. Simulations. Numerical results

As we have pointed out previously, our main interest regarding the FORC diagrams, is to know the degree of accuracy on the quantitative information about the switching field distribution and interactions that is possible to obtain for nanoparticle systems.

For that reason, starting from Eq. (11) we performed numerical simulations to study the degree of accuracy of the model. In our description this accuracy is related to the fact that $\frac{\partial\gamma(\tilde{H}_0)}{\partial H_0}$ is approximated by a delta distribution.

Our first test was carried out using a gaussian distribution of K and h_i (with $<h_i> = 0$) and a lognormal distribution for ϕ. In all calculations related to the FORC diagrams, it has been used the reduced fields $h=H/<H_A>$ normalized to the average value of the anisotropy field $<H_A>$ and normalize the FORC density in order to reach the unity as the maximum value.

As we are dealing with a nanoparticle system, the temperature plays a crucial role on the magnetic behavior. Then it is very useful to define the Δ parameter, which relates the energy barrier with the experimental measurement time and the thermal energy, as follow:

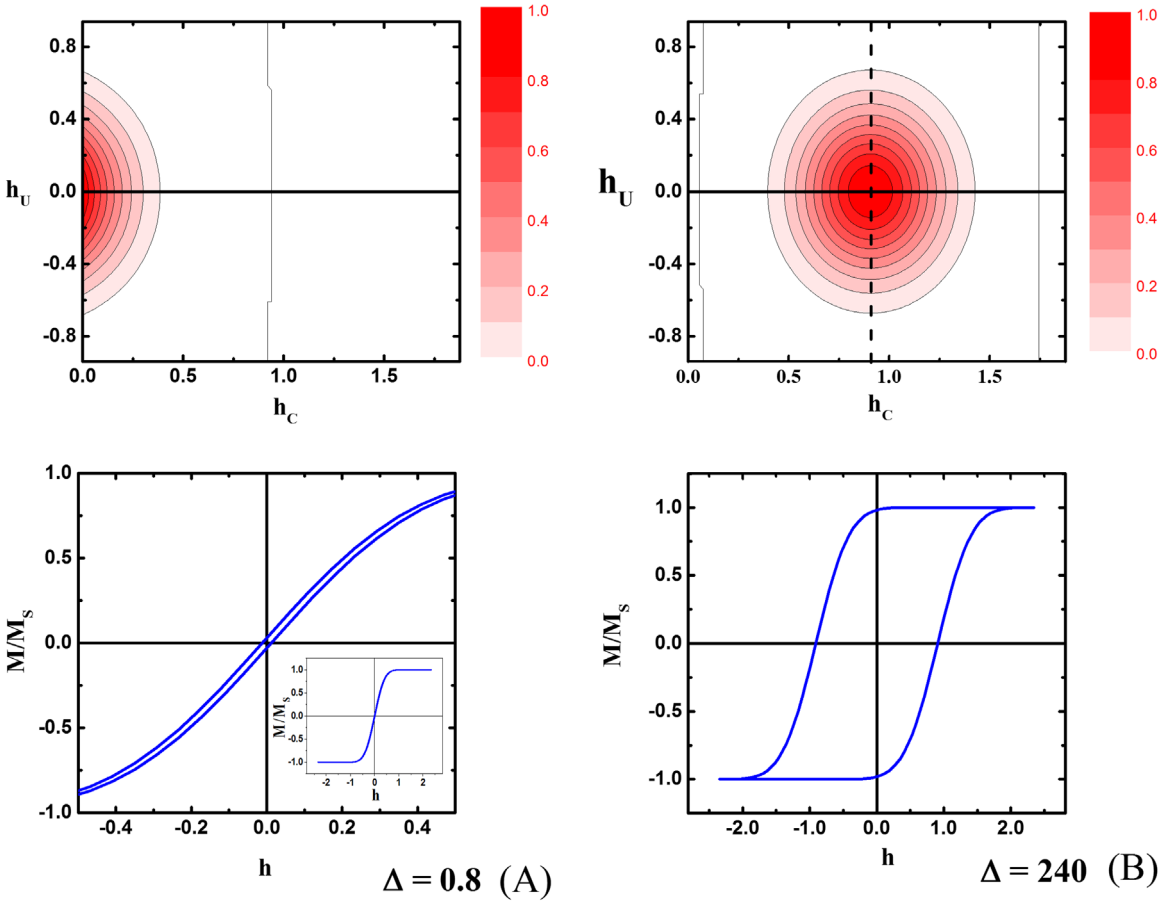

Fig. 2. Simulated FORC diagrams and hysteresis loops for $\Delta=240$ (a) and $\Delta=0.8$ (b). Bottom panels: hysteresis loops associated to the correspondent FORC diagrams. $h=H/<H_A>$ is the reduced field.

$$\Delta=\frac{<K><V>}{k_BT\ln(4\tau_m/\tau_0)} \tag{12}$$

We can associate Δ^{-1} to a reduced temperature scale, where Δ values close to 1 represents high temperatures, and $\Delta \gg 1$ corresponds to low temperatures.

In order to compare two representative cases we plot in Fig. 2 the FORC diagrams and the hysteresis loops for high (a) and low (b) temperatures.

On the high temperature case, we observe a narrow coercive fields distribution with a mean value close to zero. On the other hand, for the low temperature case, we have a FORC diagram centered on a mean h_c value well above zero and slightly wider than the high temperature one. This is directly reflected on the squarness of the hysteresis loop showed on the bottom part of Fig. 2(b).

Concerning the interaction field distribution, which is related to the vertical axis of the FORC diagram, in Fig. 2 we can observe that both cases have similar features. Regarding these diagrams, we want to highlight a particular point about their properties. Different profiles taken at constant h_u or h_c have translation symmetry along their own axis. This symmetry comes from the factorized expression obtained in Eq. (11).

In order to quantify the accuracy of the h_i and h_c distributions, we show in Fig. 3 two profiles of the FORC diagrams at different temperatures. On the left panel (Fig. 3(a)), it is shown a $\tilde{h}_u$ profile obtained at constant $\tilde{h}_c$ across the maximum value of the distribution, and, on the right panel it is shown a $\tilde{h}_c$ profile obtained at constant $\tilde{h}_u$.

The open symbols correspond to the data of Fig. 2, while the solid lines are the expected theoretical distributions given by:

$$\begin{cases} f_{H_c}(\tilde{h}_c) = \dfrac{1}{<V>}\int_{\Omega K} f_K \int_{\Omega\phi} f_\phi\, \phi^3\, \delta\left(\left|\tilde{h}_c\right| - h_c(\phi, K)\right) d\phi \\ f_{H_i}(\tilde{h}_i) = \int_{\Omega H_i} f_{H_i}\, \delta(\tilde{h}_i - h_i)\, dh_i \end{cases} \tag{13}$$

where h_c is the normalized coercive field expression given by Eq. (10).

Regarding these distributions, we remark that these definitions are consistent with those that could be obtained using the FORC distribution (Eq. (11)) and the identities given by Eq. (9). In this sense, we can assert that the definitions of Eq. (13) are compatible with the Presiach model description.

In order to obtain numerical results for Eq. (13) it is necessary to approximate the delta distributions. In this work we choose to use the numerical derivative of an approximation of the Heaviside step distribution given by $\theta(x) \approx 1/\left(1+e^{-\alpha x}\right)$ (with $\alpha = 2000$).

It is remarkable the good agreement between the profiles obtained by using the FORC information and the expected distributions of Eq. (13).

To quantify the accuracy of the profiles obtained by using the FORC diagrams, we define a confidence factor C, which compare the FORC profiles with the expected results of Eq. (13), as follow:

$$C=1-\frac{\int_{-\infty}^{\infty}|f(x)-G(x)|dx}{\int_{-\infty}^{\infty}f(x)dx} \tag{14}$$

where $f(x)$ is the expected distribution function and $G(x)$ is the

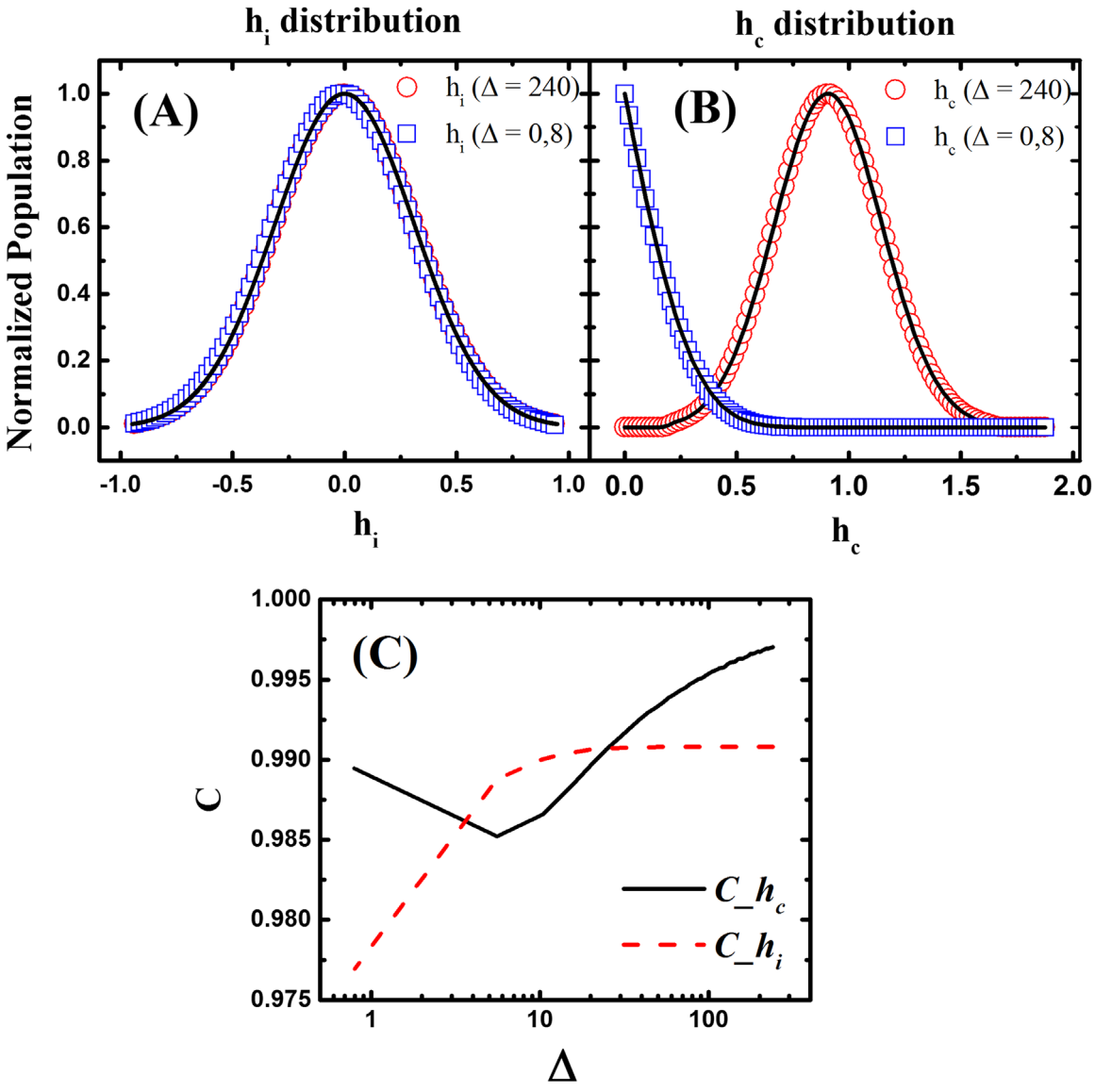

Fig. 3. h_i (panel (A)) and h_c (panel (B)) profile distributions corresponding to data of Fig. 2. Dots correspond to the FORC data, lines to definitions given in Eq. (13). Panel (C) shows the evolution of the C confidence coefficients (associated to h_c and h_i) with the Δ control parameter.

probe function. As the C value approximate to 1, the $G(x)$ distribution becomes close to $f(x)$. This parameter becomes highly relevant to quantify the range of validity of our results.

In Fig. 3(c) it is presented the confidence factor C for h_i and h_c distributions at different temperatures. We can see in both cases that the agreement between FORC profiles and the expected distributions is higher than 97 % even at the high temperature regime.

Up to now all the results discussed in this work correspond to a particular election of the h_i, K, and ϕ distributions. In order to study, how the election of a particular profile for the parameters (h_i, K, and ϕ) affect the h_i and h_c data obtained from FORC diagrams, we calculate them using normal, lognormal, triangular and uniform distributions for the anisotropy, interaction field and diameter. It is well known that some of the chosen distributions are highly pathological, but we want to emphasize that the main objective is to test the robustness of the model even in the worst scenarios.

As it was shown in Fig. 3 it is expected that the obtained h_i distribution does not depend on temperature. For this reason, the calculated profile from Eq. (11) is the same that the input h_i distribution given by the Eq. (13). In contrast, the coercive field distribution h_c, also shown in Fig. 3, has a marked thermal dependence. Then, we studied the h_c profile in the low temperature regime using $\Delta=240$.

In Fig. 4 we present several h_c profiles corresponding to different K and ϕ distributions. Each panel of Fig. 4 corresponds to normal (A), lognormal (B), triangular (C) and uniform (D) K distributions where each kind of symbols correspond to a particular ϕ distribution as it is indicated by the labels on panel (B). The simulations were performed considering $\Delta=240$, $\sigma_V/<V>=0.66$, and $\sigma_K/<K>=0.31$. It is evident some particular characteristics that we want to remark as follow. First, in all the cases the obtained h_c profile inherits the K distribution profile. This fact can be understood considering the Eq. (10), which corresponds to the thermal evolution of the coercive field. This expression shows clearly that at very low temperatures (or large Δ values) the profile of the h_c distribution must be identical (corrected by the factor $2/M_s$) to the K distribution. It is important to emphasize that the diameter profile (ϕ) distribution has not a relevant role in the h_c profiles shown in Fig. 4. However, it is important to remark that to obtain the good agreement shown in Fig. 4, we used different kind of distributions but always with the same values of mean volume ($<V>$) and its dispersion (σ_V). This can be understood in terms of

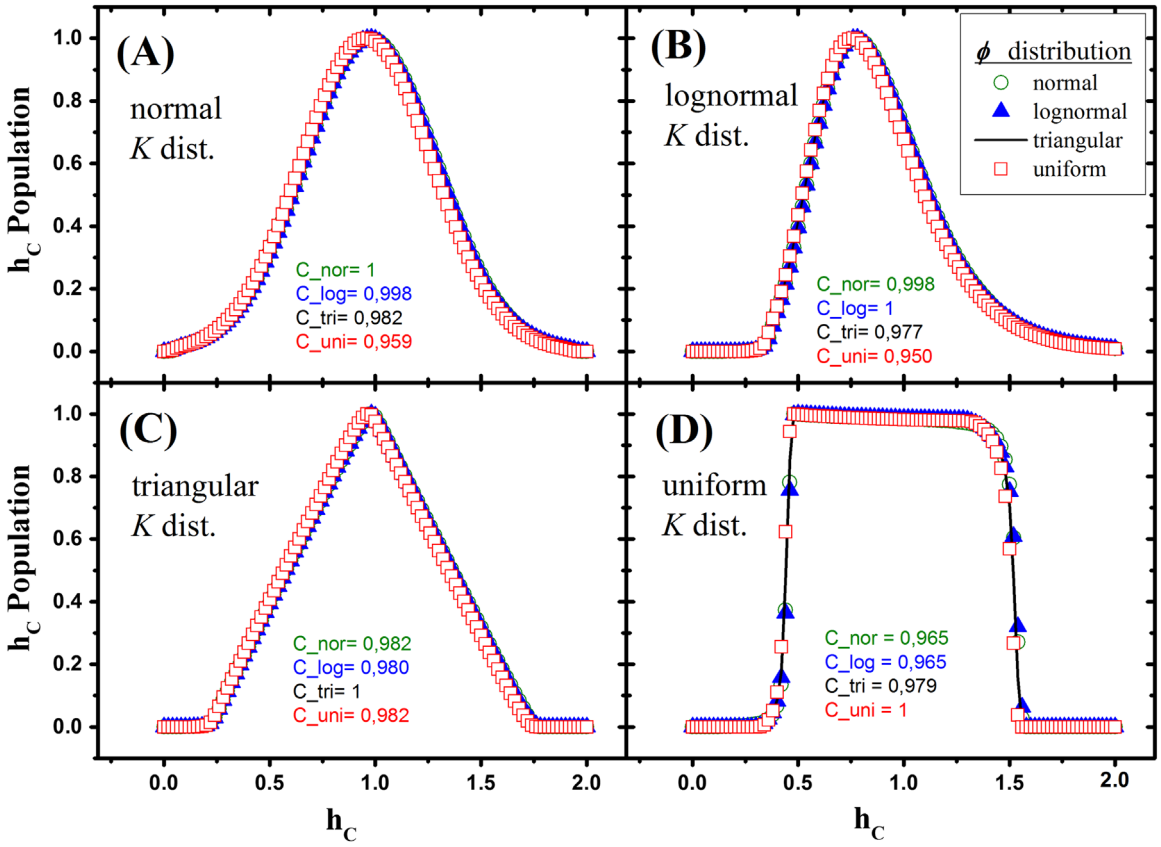

Fig. 4. h_c profiles obtained for normal (A), lognormal (B), triangular (C), and uniform (D) K distribution. In all cases $\Delta=240$, $\sigma_K/<K>=0.31$, and $\sigma_V/<V>=0.66$. The size distributions are represented by different kinds of dots and lines.

the fact that in (Eqs. (11) and 13) the quantity relevant is the volume and not the diameter, because the magnetization is proportional to the last one.

As shown in Fig. 4, the coincidence between the profiles of different diameters distributions is better than 95 % in all cases (see the confidence factor C on each panel). Note that $C=1$ corresponds to compare any of the profile distributions with itself. These results lead to the conclusion that, if we fit the profiles of Fig. 4 (using Eq. (13)) with the appropriate K distribution, we can get information about this, but not about the diameters distribution; we can only can get information about $<V>$ and σ_V.

From the results showed in Fig. 4 we can infer, almost trivially, the shape of the K distribution, but it is important to remark that it was always on the low temperature limit ($\Delta=240$). Then, on the next paragraph, we will address how we can deal with the system at higher temperatures.

On the one hand we want to quantify how accurate is the "similarity" between the distributions of h_c and K as a function of temperature. Also, we want to know the degree of accuracy on the estimation of the anisotropy distribution from FORC diagrams.

In the limit of $T\to 0(\Delta\to\infty)$, the Eq. (10) indicates that the h_c distribution must be, except for a scale factor, identically to the K one and $\sigma_{h_c}/<h_c>=\sigma_K/<K>$. In contrast, as the temperature increase, the $\sigma_{h_c}/<h_c>$ ratio is modified by thermal effects and the volume distribution.

Fig. 5 shows h_c distribution profiles as a function of h, calculated using different K distributions: normal (A), lognormal (B), triangular (C) and uniform (D). Focusing our attention on the triangular K distribution, we can see on panel (C) two profiles of h_c at different temperatures obtained from FORC diagrams simulations with $\Delta=250$ (open circles) and $\Delta=1$ (open stars). The profile obtained in the low temperature regime is almost the same as shown before in Fig. 4 (C), but when temperature increases the shape of the profile strongly change losing their triangular appearance, despite of K distribution remains the same. In order to study the effect of temperature, we calculate $<h_c>$ and σh_c values from the data of Fig. 5, and built a triangular distribution with these parameters, to be used as a reference (showed in solid and dashed lines). As the low temperature profile obtained from FORC diagrams is almost triangular, it is evident that the built distribution is almost the same to the obtained from the FORC. In contrast on the high temperature regime we can see major differences. However these differences, we remark that triangular and uniform distributions are highly pathological.

The fact that the shape of K distribution is not reflected on the h_c profile at high temperature is observed for all the studied distributions. In order to quantify the difference between the h_c distribution obtained from the FORC profile and the reference distribution, we calculate the C confidence factor between both. In Fig. 6A we present the evolution of C as a function of Δ, for different K distributions. For $\Delta\geq 30$, except the pathological uniform distribution, the discrepancy between the reference and the h_c distributions is less than 10%.

Usually, the main interest is to have information about the K distribution, assuming the previous knowledge of their "shape". In other words, if we know the profile distribution of K, how well could be estimated the ratio $\sigma_K/<K>$ from the h_c distribution data as function of temperature. With this in mind, we define the quantity

$$\Gamma = 1-\frac{\left|\frac{\sigma_{h_c}}{h_c}-\frac{\sigma_K}{K}\right|}{\frac{\sigma_K}{K}} \qquad (15)$$

where Γ indicates the relative coincidence between the σ_{h_c}/h_c and

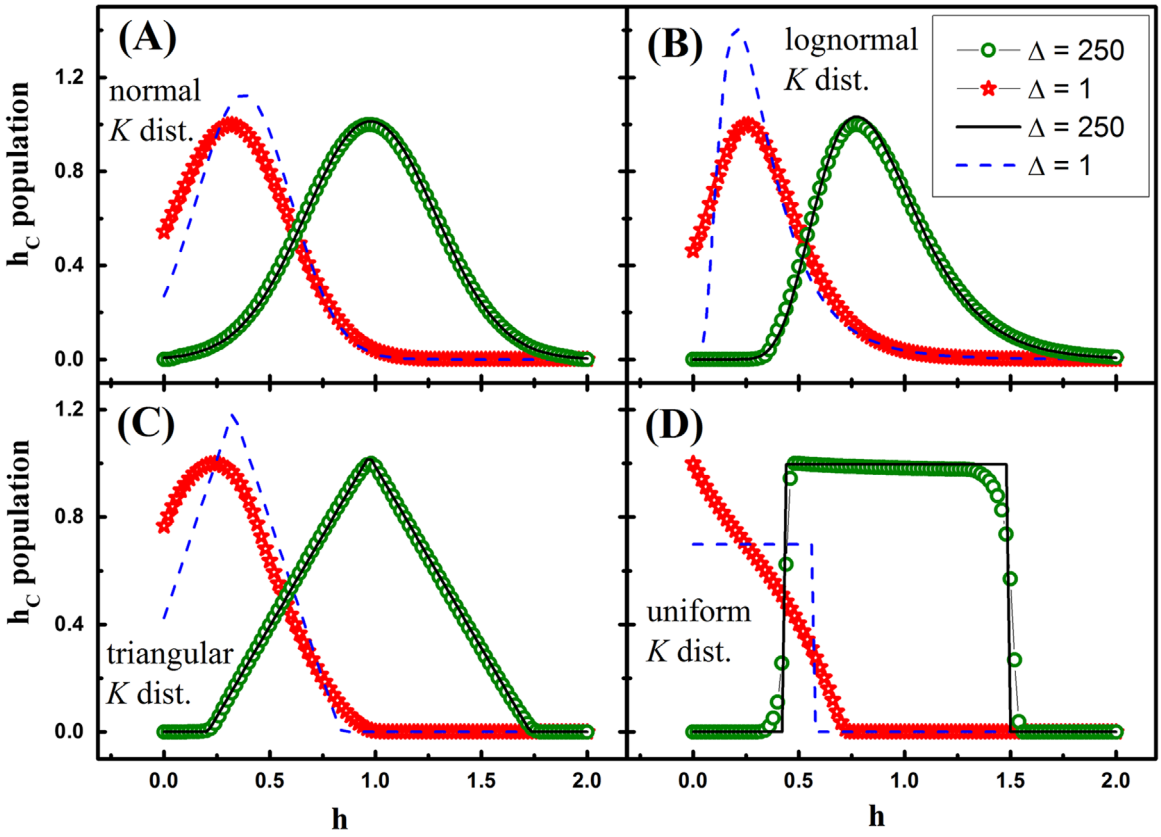

Fig. 5. h_c distributions profiles for $\Delta=250$ (open circles) and $\Delta=1$ (open starts). The lines correspond to the same kind of K distribution in each case, with the same mean value and dispersion that the FORC h_c profiles.

σ_K/K ratios. In Fig. 6 (B) we present the evolution of Γ as function of Δ for each of the K distributions. The dashed horizontal line represents the unit, i.e. the case limit case when σ_{h_c}/h_c and σ_K/K match exactly. The figure shows an almost universal curve behavior, i.e., independent of the used K distribution. Particularly, for $\Delta\to\infty$ the ratio $\sigma_{h_c}/\langle h_c\rangle$ tends to 1. From data of Fig. 6 (B) we observed that, for $\Delta\sim50$ the error in the estimation of $\sigma_K/\langle K\rangle$ is close to 13%, and for $\Delta\sim250$ value is around 3%.

Using the fact that Γ exhibits an approximately universal behavior, independent of the profile of K distribution, we want to find an expression for this. Then, considering the anisotropy, volume and its dispersion, as well as Δ, we calculated $\sigma h_c/\langle h_c\rangle$ starting from Eq. (10), using the definition (12), and assuming that the dispersion σh_c comes from the quadratic square root of the sum of quadratic contribution of K, and $\langle V\rangle$. Making a Taylor series expansion at order $\Delta^{-1/2}$ (low temperature limit), we obtain:

$$\begin{cases}\dfrac{\sigma h_c}{\langle h_c\rangle}\approx\dfrac{\sigma K}{\langle K\rangle}\left(1+\dfrac{1}{2\sqrt{\Delta}}\right)\\ \Gamma\approx 1-\dfrac{1}{2\sqrt{\Delta}}\end{cases}\qquad(16)$$

The dash line in Fig. 6(b) corresponds to the curve descript by Eq. (16). It is noticeable that the asymptotic approximation is outstanding. Remarkably, the correction given by the volume distribution does not appears at order $\Delta^{-1/2}$. This means that for "sufficiently" large values of Δ, the volume correction can be neglected. Combining (Eqs. (16) and 12) we can estimated the degree of accuracy in the direct estimation of $\sigma_K/\langle K\rangle$ from $\sigma_{h_c}/\langle h_c\rangle$. For example, for a desirable estimation of $\sim$5% should be enough taking $\Delta=100$. Converting $\Delta=100$ value to temperature values depends of the characteristic parameters of each system. For instance, considering the case of a normal distribution of anisotropy with a mean value of 8×10^5 erg/cm^3, and a lognormal size distribution given by ϕ_0=15nm and $\sigma=0.4$, then $\Delta=100$ corresponds to $T=7$ K [29]. If Calculating the same system measured at 80 K, for instance, we obtain $\Gamma\sim0.5$ which is a poor estimation, however for ϕ_0=20nm in the same experimental conditions $\Gamma\sim0.7$.

As a final remark, due the fact that Eq. (11), by the simplifications and assumption, can be "associated" to the Preisach–Néel model, and the definitions given in (13) to the Preisach model, could be claim that the spirit of the work results in the analysis of a comparison between the distributions of h_c and h_i associated to both models.

3. Conclusions

In this work we have studied the degree of accuracy of the information obtained using the FORC diagrams for a nanoparticle system. We developed an analytical model describing the FORC diagram as function of the applied external field, the experimental time windows and temperature. In the model it is assumed that the easy axes of the particles are all oriented along the $\vec{H}$ direction and also the interactions fields are not dependent of the state of the magnetization. Defining the irreversibility and interactions fields distributions as a function of temperature, volume distribution, anisotropy, and other parameters, we were able to quantify the degree of accuracy of the information obtained from these diagrams. The results of the simulations indicate that this is a very appropriate and accurate technique. The description of the distributions of the irreversibility and interactions fields is outstanding, even for the case of high temperatures ($\Delta\sim1$). However, we verified that increasing the temperature qualitative and quantitative information about distributions in the system are losing.

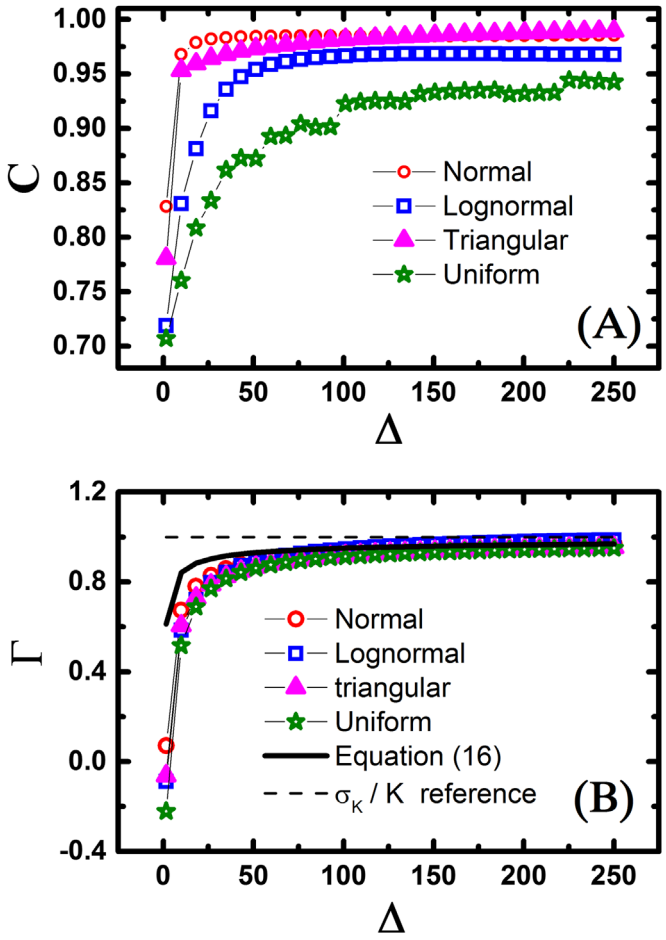

Fig. 6. Upper panel: C coefficient relating the dots and lines of Fig. 5 as function of Δ. $\Delta \geq 30$ the agreement is superior that 90 % (at exception of the uniform distribution, which needs $\Delta \geq 75$). Bottom panel: dots corresponds to Γ data, dashed lines indicates the reference value, and the solid line the asymptotical expression of Eq. (16).

It was found that the distribution shape of coercive fields is determined principally by the distribution of anisotropy, especially at low temperatures ($\Delta \gg 1$); the role played by the size distribution is reduced. Only the volume average and its dispersion values are relevant, regardless the shape of the size distribution. Our results also indicate that for $\Delta \sim 50$ the shape of K distribution can be obtained with a good accuracy (over 90%) from the $\Delta \sim 50$ profile (except for pathological cases as the uniform distribution, in which case $\Delta \sim 100$ is required). In addition, at very low temperatures $\Delta \sim 100$ it is possible estimate the $\sigma K/\langle K \rangle$ ratio with a high degree of confidence (95%) directly from the h_c FORC distribution profile.

Acknowledgments

This work is part of a research project supported by Agencia Nacional de Promoción Científica y Tecnológica (Argentina), under Grants No. PICT-2012-0492 and PICT-2012-2995, CONICET under Grant No. PIP 201101-519, and Universidad Nacional de Cuyo under Grants 06/C006, 06/C464 and 06/C427.

References

[1] C.-I. Dobrota, A. Stancu, Tracking the individual magnetic wires' switchings in ferromagnetic nanowire arrays using the first-order reversal curves (FORC) diagram method, Phys. B Condens. Matter 457 (2015) 280.
[2] S. Samanifar, M. Almasi Kashi, A. Ramazani, M. Alikhani, Reversal modes in FeCoNi nanowire arrays: Correlation between magnetostatic interactions and nanowires length, J. Magn. Magn. Mater. 378 (2015) 73.
[3] M. Almasi-Kashi, a Ramazani, M. Amiri-Dooreh, FORC investigation of as-deposited and annealed CoZn alloy nanowires, Phys. B Condens. Matter 452 (2014) 124.
[4] D. a Gilbert, et al., Quantitative decoding of interactions in tunable nanomagnet arrays using first order reversal curves, Sci. Rep. 4 (2014) 4204.
[5] J.C. Martínez-García, M. Rivas, D. Lago-Cachón, J. a García, First-order reversal curves analysis in nanocrystalline ribbons, J. Phys. D: Appl. Phys. 47 (2014) 015001.
[6] M. Pan, P. Zhang, H. Ge, N. Yu, Q. Wu, First-order-reversal-curve analysis of exchange-coupled SmCo/NdFeB nanocomposite alloys, J. Magn. Magn. Mater. 361 (2014) 219.
[7] M.P. Proenca, J. Ventura, C.T. Sousa, M. Vazquez, J.P. Araujo, Angular first-order reversal curves: an advanced method to extract magnetization reversal mechanisms and quantify magnetostatic interactions, J. Phys. Condens. Matter 26 (2014) 116004.
[8] a Ramazani, M. Almasi Kashi, a H. Montazer, Fabrication of single crystalline, uniaxial single domain Co nanowire arrays with high coercivity, J. Appl. Phys. 115 (2014) 113902.
[9] M. Almasi-Kashi, a Ramazani, E. Golafshan, M. Arefpour, E. Jafari-Khamse, First order reversal curve investigation of the hard and soft magnetic phases of annealed CoFeCu nanowire arrays, Phys. B Condens. Matter 429 (2013) 46.
[10] M.P. Proenca, et al., Magnetic interactions and reversal mechanisms in Co nanowire and nanotube arrays, J. Appl. Phys. 113 (2013) 093907.
[11] T. Schrefl, et al., First order reversal curve studies of permanent magnets, J. Appl. Phys. 111 (2012) 07A728.
[12] A. Rotaru, et al., Interactions and reversal-field memory in complex magnetic nanowire arrays, Phys. Rev. B 84 (2011) 134431.
[13] C.-I. Dobrota, A. Stancu, What does a first-order reversal curve diagram really mean? A study case: Array of ferromagnetic nanowires, J. Appl. Phys. 113 (2013) 043928.
[14] M. Knobel, et al., Superparamagnetism and other magnetic features in granular materials: a review on ideal and real systems, J. Nanosci. Nanotechnol. 8 (2008) 2836.
[15] Lima Jr., et al., Relaxation time diagram for identifying heat generation mechanisms in magnetic fluid hyperthermia, J. Nanopart. Res. 16 (2014) 2791.
[16] E. Lima, et al., Heat generation in agglomerated ferrite nanoparticles in an alternating magnetic field, J. Phys. D: Appl. Phys. 46 (2013) 045002.
[17] J. Yin, H. Zhang, F. Hu, B. Shen, L.Q. Pan, First order reversal curve diagrams of perpendicular magnetic anisotropy films, J. Appl. Phys. 106 (2009) 103901.
[18] T. Maurer, et al., Magnetic nanowires as permanent magnet materials, Appl. Phys. Lett. 91 (2007) 96.
[19] Preisach, Füber die magnetische Nachwirkung, Z. für Phys. 94 (1935) 277–302.
[20] L.G. Vivas, et al., Magnetic anisotropy in CoNi nanowire arrays: Analytical calculations and experiments, Phys. Rev. B 85 (2012) 035439.
[21] A. Stancu, C. Pike, L. Stoleriu, P. Postolache, D. Cimpoesu, Micromagnetic and Preisach analysis of the First Order Reversal Curves (FORC) diagram, J. Appl. Phys. 93 (2003) 6620.
[22] A. Stancu, et al., Investigation of the switching characteristics in ferroelectrics by first-order reversal curve diagrams, Phys. B Condens. Matter 372 (2006) 226.
[23] C. Pike, First-order reversal-curve diagrams and reversible magnetization, Phys. Rev. B 68 (2003) 104424.
[24] C.R. Pike, A.P. Roberts, K.L. Verosub, Characterizing interactions in fine magnetic particle systems using first order reversal curves, J. Appl. Phys. 85 (1999) 6660.
[25] E. De Biasi, R.D. Zysler, C.A. Ramos, M. Knobel, A new model to describe the crossover from superparamagnetic to blocked magnetic nanoparticles, J. Magn. Magn. Mater. 320 (2008) 312.
[26] A.R. Muxworthy, D.J. Dunlop, First-order reversal curve (FORC) diagrams for pseudo-single-domain magnetites at high temperature, Earth Planet. Sci. Lett. 203 (2002) 369.
[27] L. Spinu, A. Stancu, Modelling magnetic relaxation phenomena in fine particle systems with a Presiach-Néel model, J. Magn. Magn. Mater. 189 (1998) 106.
[28] I. Borcia, L. Spinu, A. Stancu, Simulation of magnetization curves with Presiach-Néel models, J. Magn. Magn. Mater. 242-245 (2002) 1034.
[29] The calculation is Performed Using Equation 12 and Assuming $\tau_m \sim 100$ s and $\tau_0 \sim 10^{-10}$ s.